Available online at www.sciencedirect.com
SCIENCE DIRECT®
International Journal of Heat and Mass Transfer 47 (2004) 1347–1359
International Journal of HEAT and MASS TRANSFER
www.elsevier.com/locate/ijhmt

Optimally staggered finned circular and elliptic tubes in forced convection

R.S. Matos [a], J.V.C. Vargas [a,*], T.A. Laursen [b], A. Bejan [c]

[a] Departamento de Engenharia Mecânica, Centro Politécnico, Universidade Federal do Paraná, Caixa Postal 19011, Curitiba, PR 81531-990, Brazil

[b] Department of Civil and Environmental Engineering, Duke University, Durham, NC 27708-0287, USA

[c] Department of Mechanical Engineering & Materials Science, Duke University, Durham, NC 27708-0300, USA

Received 14 February 2003; received in revised form 7 August 2003

Abstract

This work presents a numerical and experimental geometric optimization study to maximize the total heat transfer rate between a bundle of finned or non-finned tubes in a given volume and a given external flow both for circular and elliptic arrangements, for general staggered configurations. The optimization procedure started by recognizing the design limited space availability as a fixed volume constraint. The experimental results were obtained for circular and elliptic configurations with a fixed number of tubes (12), starting with an equilateral triangle configuration, which fitted uniformly into the fixed volume with a resulting maximum dimensionless tube-to-tube spacing $S/2b = 1.5$, where S is the actual spacing and b is the smaller ellipse semi-axis. Several experimental configurations were built by reducing the tube-to-tube spacings, identifying the optimal spacing for maximum heat transfer. Similarly, it was possible to investigate the existence of optima with respect to other two geometric degrees of freedom, i.e., tube eccentricity and fin-to-fin spacing. The results are reported for air as the external fluid, in the range $852 \leqslant Re_L \leqslant 8520$, where L is the swept length of the fixed volume. Circular and elliptic arrangements with the same flow obstruction cross-sectional area were compared on the basis of maximum total heat transfer. This criterion allows one to quantify the heat transfer gain in the most isolated way possible, by studying arrangements with equivalent total pressure drops independently of the tube cross-section shape. The first part of the paper reports two-dimensional numerical optimization results for non-finned circular and elliptic tubes arrangements, which are validated by direct comparison with experimental measurements with good agreement. The second part of the paper presents experimental optimization results for non-finned and finned circular and elliptic tubes arrangements. A relative heat transfer gain of up to 20% is observed in the optimal elliptic arrangement, as compared to the optimal circular one. Both local optimal eccentricity ($S/2b = 0.25$ and fixed fin-to-fin spacing) and local optimal fin-to-fin spacing (circular tube and $S/2b = 0.5$) are shown to exist. Such findings motivate the search for global optima with respect to tube-to-tube spacing, eccentricity and fin-to-fin spacing in future three-dimensional numerical optimization studies.

1. Introduction

The optimization of industrial processes for maximum utilization of the available energy (exergy) has been a very active line of scientific research in recent times. The increase in energy demand in all sectors of the human society requires an increasingly more intelligent use of available energy. Many industrial applications require the use of heat exchangers with tubes arrangements, either finned or non-finned, functioning as heat exchangers in air conditioning systems, refrigeration, heaters, radiators, etc. Such devices have to be designed according to the availability of space in the device containing them. A measure of the evolution of such equipment, therefore, is the reduction in size, or in

* Corresponding author. Tel.: +55-41-361-3307; fax: +55-41-361-3129.
E-mail address: jvargas@demec.ufpm.br (J.V.C. Vargas).

0017-9310/$ - see front matter © 2003 Elsevier Ltd. All rights reserved.
doi:10.1016/j.ijheatmasstransfer.2003.08.015

Nomenclature

a	larger ellipse semi-axis (m)
A_c	minimum free flow cross-sectional area (m^2)
b	smaller ellipse semi-axis (m)
B_a	bias limit of quantity a
c_p	fluid specific heat at constant pressure (J/(kg K))
D	tube diameter (m)
e	ellipses eccentricity, b/a
H	array height (m)
k	fluid thermal conductivity (W/(m K))
L	array length (m)
$L/2b$	array length to smaller ellipses axis aspect ratio
$\dot{m}_{ec}$	fluid mass flow rate entering one elemental channel (kg/s)
n_f	number of fins
N	number of tubes in one unit cell
N_{ec}	number of elemental channels
p	pressure (N/m^2)
P	dimensionless pressure
Pe_L	Peclet number based on array length
Pr	fluid Prandtl number, v/α
P_a	precision limit of quantity a
$\tilde{q}$	dimensionless overall thermal conductance, Eq. (13)
$\tilde{q}_*$	dimensionless overall thermal conductance, Eq. (17)
Q	overall heat transfer rate (W)
Q_{ec}	heat transfer rate of one elemental channel (W)
Re_D	Reynolds number based on tube diameter, $u_\infty D/v$
Re_L	Reynolds number based on array length, $u_\infty L/v$
Re_δ	Reynolds number based on fin-to-fin spacing, $u_\infty \delta/v$
S	spacing between rows of tubes (m), Fig. 1
S/D	dimensionless spacing between rows of tubes (circular arrangement)
$S/2b$	dimensionless spacing between rows of tubes (elliptic arrangement)
t	fin thickness (m)
t	time (s)
T	temperature (K)
$\overline{T}$	average fluid temperature (K)
u, v, w	velocity components (m/s)
U, V, W	dimensionless velocity components
U_a	uncertainty of quantity a
W	array width (m)
x, y, z	cartesian coordinates (m)
X, Y, Z	dimensionless cartesian coordinates

Greek symbols

α	thermal diffusivity (m^2/s)
ε	mesh convergence criterion, Eq. (19)
δ	fin-to-fin spacing (m)
θ	dimensionless temperature
$\bar{\theta}$	dimensionless average fluid temperature
v	fluid kinematic viscosity (m^2/s)
ρ	density (kg/m^3)
ϕ_f	dimensionless fin density in direction z

Subscripts

max	maximum
opt	optimal
out	unit cell outlet
w	tube surface
∞	free stream

occupied volume, accompanied by the maintenance or improvement of its performance. Hence, the problem consists of identifying a configuration that provides maximum heat transfer for a given space [1].

Heat exchangers with finned elliptical tubes were studied experimentally by Brauer [2], Bordalo and Saboya [3], Saboya and Saboya [4], and Jang and Yang [5] showing that besides the relative heat transfer gain observed in the elliptical arrangements, as compared to the circular ones, a relative pressure drop reduction of up to 30% was observed. Rocha et al. [6] developed a hybrid mathematical model for finned circular and elliptic tubes arrangements based on energy conservation and on heat transfer coefficients obtained experimentally by a naphthalene sublimation technique through a heat and mass transfer analogy [4,7], and obtained numerically the fin temperature distribution and fin efficiency in one and two row elliptic tube and plate fin heat exchangers. The fin efficiency results were then compared with the results of Rosman et al. [8] for plate fin and circular heat exchangers, and a relative fin efficiency gain of up to 18% was observed with the elliptical arrangement.

Recently, Bordalo and Saboya [3] reported pressure drop measurements comparing elliptic and circular tube and plate fin heat exchanger configurations, with one-, two- and three-row arrangements. Reductions of up to 30% of the loss coefficient (pressure drop coefficient per unit row due only to the presence of the tubes) were observed, in favor of the elliptic configuration. The comparison was performed between circular and elliptic arrangements with the same flow obstruction cross-sectional area, for $200 \leqslant Re_\delta \leqslant 2000$ ($1.8\ m/s \leqslant u_\infty \leqslant 18.2\ m/s$, with $\delta = 1.65$ mm), which cover the air velocity range of interest for air conditioning applications. It is

further observed that the reduction in pressure drop is higher as Re_δ increases and negligible for $Re_\delta \sim 200$, for the three-row arrangement.

The present study is a natural 'next step' following the work presented by Matos et al. [9], where a two-dimensional (2-D) heat transfer analysis was performed in non-finned circular and elliptic tubes heat exchangers. The finite element method was used to discretize the fluid flow and heat transfer governing equations and a 2-D isoparametric, four-noded, linear element was implemented for the finite element analysis program, FEAP [10]. The numerical results for the equilateral triangle staggering configuration, obtained with the new element were then validated qualitatively by means of direct comparison to previously published experimental results for circular tubes heat exchangers [11]. Numerical geometric optimization results showed a relative heat transfer gain of up to 13% in the optimal elliptical arrangement, as compared to the optimal circular one. The heat transfer gain and the relative pressure drop reduction of up to 30% observed in previous studies [2–5] show that the elliptical arrangement has the potential for a considerably better overall performance than the traditional circular one.

The main focus of this work is on the experimental geometric optimization of staggered finned circular and elliptic tubes in a fixed volume. In the first part of the paper, a 2-D numerical optimization procedure for non-finned circular and elliptic arrangements is conducted and validated by means of direct comparison to experimental measurements. The second part of the paper describes a series of experiments conducted in the laboratory in the search for optimal geometric parameters in general staggered finned circular and elliptic configurations for maximum heat transfer. Circular and elliptic arrangements with the same flow obstruction cross-sectional area are then compared on the basis of maximum total heat transfer. Appropriate non-dimensional groups are defined and the optimization results reported in dimensionless charts.

2. Theory

A typical four-row tube and plate fin heat exchanger with a general staggered configuration is shown in Fig. 1. Fowler and Bejan [12] showed that in the laminar regime, the flow through a large bank of cylinders can be simulated accurately by calculating the flow through a single channel, such as that illustrated by the unit cell seen in Fig. 1. Because of the geometric symmetries, there is no fluid exchange or heat transfer between adjacent channels, or at the top and side surfaces. At the bottom of each unit cell, no heat transfer is expected

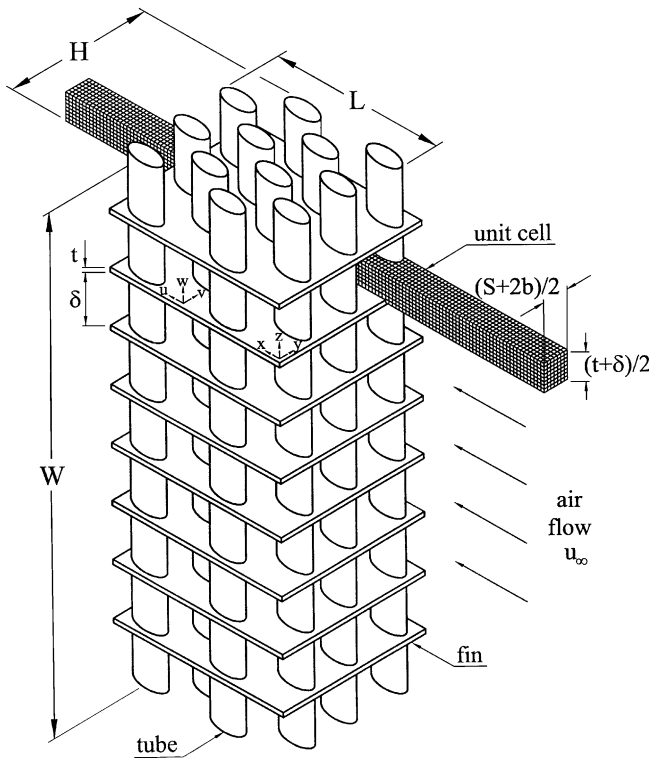

Fig. 1. Arrangement of finned elliptic tubes, and the three-dimensional computational domain.

across the plate fin midplane. In Fig. 1, L, H and W are the length, height and width (tube length) of the array, respectively. The fins are identical, where t is the thickness and δ is the fin-to-fin spacing.

The governing equations are the mass, momentum and energy equations which were simplified in accordance with the assumptions of three-dimensional incompressible steady-state laminar flow with constant properties, for a Newtonian fluid [13]:

$$\frac{\partial U}{\partial X}+\frac{\partial V}{\partial Y}+\frac{\partial W}{\partial Z}=0 \tag{1}$$

$$U\frac{\partial U}{\partial X}+V\frac{\partial U}{\partial Y}+W\frac{\partial U}{\partial Z} =-\frac{\partial P}{\partial X}+\frac{1}{Re_{\mathrm{L}}}\left[\frac{\partial^2 U}{\partial X^2}+\frac{\partial^2 U}{\partial Y^2}+\frac{\partial^2 U}{\partial Z^2}\right] \tag{2}$$

$$U\frac{\partial V}{\partial X}+V\frac{\partial V}{\partial Y}+W\frac{\partial V}{\partial Z} =-\frac{\partial P}{\partial Y}+\frac{1}{Re_{\mathrm{L}}}\left[\frac{\partial^2 V}{\partial X^2}+\frac{\partial^2 V}{\partial Y^2}+\frac{\partial^2 V}{\partial Z^2}\right] \tag{3}$$

$$U\frac{\partial W}{\partial X}+V\frac{\partial W}{\partial Y}+W\frac{\partial W}{\partial Z} =-\frac{\partial P}{\partial Z}+\frac{1}{Re_{\mathrm{L}}}\left[\frac{\partial^2 W}{\partial X^2}+\frac{\partial^2 W}{\partial Y^2}+\frac{\partial^2 W}{\partial Z^2}\right] \tag{4}$$

$$U\frac{\partial \theta}{\partial X}+V\frac{\partial \theta}{\partial Y}+W\frac{\partial \theta}{\partial Z}=\frac{1}{Pe_{\mathrm{L}}}\left[\frac{\partial^2 \theta}{\partial X^2}+\frac{\partial^2 \theta}{\partial Y^2}+\frac{\partial^2 \theta}{\partial Z^2}\right] \tag{5}$$

The symmetries present in the problem allow the solution (computational) domain to be reduced, to one unit cell, represented by the extended domain shown in Fig. 1, of height $(S/2+b)$, and width $(\delta/2+t/2)$.

In Eqs. (1)–(5), dimensionless variables have been defined based on appropriate physical scales as follows:

$$(X,Y,Z)=\frac{(x,y,z)}{L},\quad P=\frac{p}{\rho u_\infty^2} \tag{6}$$

$$(U,V,W)=\frac{(u,v,w)}{u_\infty},\quad \theta=\frac{T-T_\infty}{T_{\mathrm{w}}-T_\infty}$$
$$Re_{\mathrm{L}}=\frac{U_\infty L}{\nu}\quad\text{and}\quad Pe_{\mathrm{L}}=\frac{U_\infty L}{\alpha} \tag{7}$$

where (x,y,z) are the Cartesian coordinates (m), p the pressure (N/m^2), ρ the fluid density (kg/m^3), u_∞ the free stream velocity (m/s), (u,v,w) the fluid velocities (m/s), T the temperature (K), T_∞ the free stream temperature (K), T_{w} the tubes surface temperature (K), L the array length in the flow direction (m), ν the fluid kinematic viscosity (m^2/s) and α is the fluid thermal diffusivity (m^2/s).

The solution domain of Fig. 1 is composed by the external fluid and half of the solid fin. The solid–fluid interface is included in the solution domain such that mass, momentum and energy are conserved throughout the domain. Eqs. (1)–(5) model the fluid part of the domain. Only the energy equation needs to be solved in the solid part of the domain, accounting for the actual properties of the solid material. The dimensionless energy equation for the solid fin is written as

$$\frac{\partial \theta}{\partial \tau}=\frac{1}{Re_{\mathrm{L}}}\frac{\alpha_{\mathrm{s}}}{\nu}\left[\frac{\partial^2 \theta}{\partial X^2}+\frac{\partial^2 \theta}{\partial Y^2}+\frac{\partial^2 \theta}{\partial Z^2}\right] \tag{8}$$

where a dimensionless time is defined by $\tau=\frac{t}{L/u_\infty}$, t is the time, and α_{s} is the solid fin thermal diffusivity (m^2/s).

For steady-state solutions $\frac{\partial\theta}{\partial\tau}$ is assumed to be zero. The solution to Eqs. (1)–(8) subject to appropriate boundary conditions for the extended domain of Fig. 1 delivers the velocities (fluid) and temperature (fluid and solid) fields.

The objective is to find the optimal geometry, such that the volumetric heat transfer *density* is maximized, subject to a volume constraint. The engineering design problem starts by recognizing the finite availability of space, i.e., an available space $L\times H\times W$ as a given volume that is to be filled with a heat exchanger. To maximize the volumetric heat transfer density means that the overall heat transfer rate between the fluid inside the tubes and the fluid outside the tubes will be maximized.

Next, the optimization study proceeds with the identification of the degrees of freedom (variables) that allow the maximization of the overall heat transfer rate between the tubes and the free stream, Q. Three geometric degrees of freedom in the arrangement are identified in this way, i.e.: (i) the spacing between rows of tubes, S; (ii) the tubes eccentricity, e; and (iii) the fin-to-fin spacing, δ. The choice of such parameters follow from the analysis of the two extremes, i.e., when they are small or large. When $S\to 0$, the mass flow rate in the elemental channel (sum of all unit cells in direction z) decreases and, therefore $Q\to 0$, and for $S\to S_{\max}$ (maximum spacing such that the arrangement with a certain number of elemental channels, N_{ec}, fits in the available space, $L\times H\times W$), the minimum free flow cross-sectional area, A_{c}, increases, thus the flow velocity decreases, the heat transfer coefficient decreases and Q decreases. When $e\to 0$, the limit of staggered flat plates is represented [14], so $Q\to Q_{\substack{\text{flat}\\\text{plates}}}$, and for $e\to 1$, the limit of circular tubes is represented [9,11], so $Q\to Q_{\substack{\text{circular}\\\text{tubes}}}$, therefore, the variation of eccentricity allows the heat transfer performance of elliptic tubes to be compared with flat plates and circular tubes, which is one of the objectives of this paper. When $\delta\to 0$, the mass flow rate in the unit cell decreases, so $Q\to 0$, and for $\delta\to\delta_{\max}=W$, the total fin surface area decreases, and Q decreases. The behavior of S, e and δ at the extremes indicate the possibility of maximum Q in the intervals, $0<S<S_{\max}$, $0<e<1$ and $0<\delta<W$.

A comparison criterion between elliptic and circular arrangements with the same flow obstruction cross-sectional area is adopted, i.e., the circular tube diameter is equal to two times the smaller ellipse semi-axis of the elliptic tube. This criterion was also adopted in previous studies [3,4,6,9]. However, the most important reason to adopt such a criterion is the possibility to obtain equivalent pressure drops in both arrangements, to be able to quantify the heat transfer gain in the most isolated way possible. As pointed out earlier in the text, the difference in pressure drop for elliptic and circular arrangements with identical flow obstruction cross-sectional areas for $Re_\delta < 200$ is negligible [3], which is also verified experimentally in the laboratory for all cases analyzed in this paper.

In this study, numerical solutions are presented only for non-finned tube arrangements. The problem can then be treated in two dimensions as shown by Matos et al. [9]. The solution domain is composed only by the external fluid in the plane x–y, with velocities u and v. The following boundary conditions are then specified for the extended 2-D computational domain of Fig. 2:

$$\text{(A)} \quad U = 1, \quad \frac{\partial V}{\partial X} = 0, \quad \theta = 0 \tag{9}$$

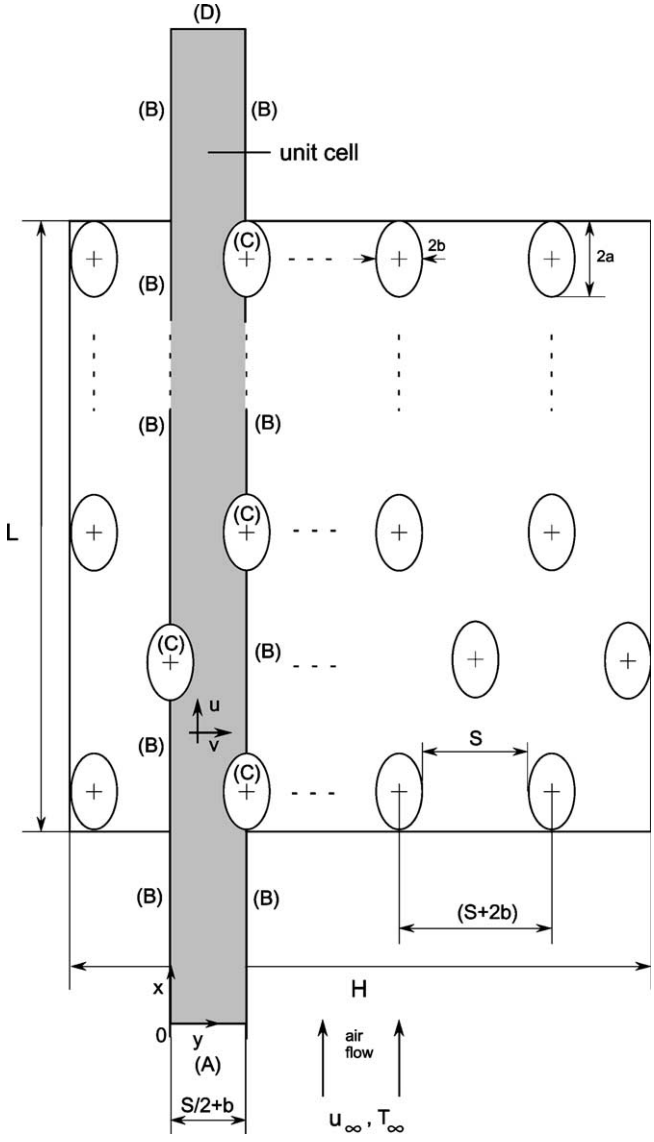

Fig. 2. Two-dimensional section through non-finned elliptic tubes and computational domain.

$$\text{(B)}\quad \frac{\partial U}{\partial Y}=0,\quad V=0,\quad \frac{\partial \theta}{\partial Y}=0 \tag{10}$$

$$\text{(C)}\quad U=V=0,\quad \theta=1 \tag{11}$$

$$\text{(D)}\quad \frac{\partial U}{\partial X}=\frac{\partial V}{\partial X}=0,\quad \frac{\partial \theta}{\partial X}=0 \tag{12}$$

In order to represent the actual flow with boundary conditions (A) and (D), two extra lengths need to be added to the computational domain, upstream and downstream, as shown in Fig. 2. The actual dimensions of these extra lengths need to be determined by an iterative numerical procedure, with convergence obtained according to a specified tolerance. Such procedure is necessary for both 2-D and 3-D simulations.

Once the geometry of the extended computational domain represented by the unit cell of Fig. 2 is specified, Eqs. (1)–(3), (5)–(7) and (9)–(12) deliver the resulting velocities, pressure and temperature fields in the domain. The dimensionless overall thermal conductance $\tilde{q}$, or volumetric heat transfer density is defined as follows [9,11]:

$$\tilde{q}=\frac{Q/(T_{\mathrm{w}}-T_{\infty})}{kLHW/(2b)^2} \tag{13}$$

where the overall heat transfer rate between the finned or non-finned tubes and the free stream, Q, has been divided by the constrained volume, LHW; k is the fluid thermal conductivity (W/(m K)) and $2b=D$ the ellipse smaller axis or tube diameter.

A balance of energy in one elemental channel states that

$$Q=N_{\mathrm{ec}}Q_{\mathrm{ec}}=N_{\mathrm{ec}}\dot{m}_{\mathrm{ec}}c_{\mathrm{p}}(\overline{T}_{\mathrm{out}}-T_{\infty}) \tag{14}$$

where N_{ec} is the number of elemental channels. The elemental channel is defined as the sum of all unit cells in direction z. Therefore, $\dot{m}_{\mathrm{ec}}=\rho u_{\infty}[(S+2b)/2](W-n_{\mathrm{f}}t)$ is the mass flow rate (kg/s) entering one elemental channel; c_{p} is the fluid specific heat at constant pressure (J/(kg K)), and $\overline{T}_{\mathrm{out}}$ is the average fluid temperature at the elemental channel outlet (K). The number of fins in the arrangement is given by

$$n_{\mathrm{f}}=\frac{W}{t+\delta} \tag{15}$$

The dimensionless overall thermal conductance is rewritten utilizing Eqs. (13)–(15),

$$\tilde{q}=\frac{N_{\mathrm{ec}}}{2}PrRe_{\mathrm{L}}\left[\frac{2b}{L}\right]^2\frac{2b}{H}\left(\frac{S}{2b}+1\right)(1-\phi_{\mathrm{f}})\bar{\theta}_{\mathrm{out}} \tag{16}$$

where $\phi_{\mathrm{f}}=\frac{n_{\mathrm{f}}t}{W}=\frac{t}{t+\delta}$, is the dimensionless fin density in direction z ($0\leqslant n_{\mathrm{f}}t\leqslant W$), and Pr the fluid Prandtl number, ν/α.

For the sake of generalizing the results of Eq. (16) for all configurations of the type studied in this work, the dimensionless overall thermal conductance is alternatively defined as follows:

$$\tilde{q}_{*}=\frac{2}{N_{\mathrm{ec}}}\left[\frac{L}{2b}\right]^2\frac{H}{2b}\tilde{q}=PrRe_{\mathrm{L}}\left(\frac{S}{2b}+1\right)(1-\phi_{\mathrm{f}})\bar{\theta}_{\mathrm{out}} \tag{17}$$

3. Numerical method

The numerical solution of Eqs. (1)–(3), (5)–(7) and (9)–(12) was obtained utilizing the finite element method [10], giving the velocities and temperature fields in the unit cell of Fig. 2. In Eqs. (1)–(3), the terms that refer to the third dimension, Z, were dropped, because only 2-D solutions for non-finned arrangements are presented in this study.

The implementation of the finite element method for the solution of Eqs. (1)–(3) and (5) starts from obtaining the variational (weak) form of the problem, as described by Reddy and Gartling [15]. The weak form is discretized with an 'upwind' scheme proposed by Hughes [16], where it is possible to adequate the discrete form of the problem to the physical characteristics of the flow. After developing the discrete form of the problem, the resulting algebraic equations are arranged in matrix form for the steady state two dimensional problem as described by Matos et al. [9].

For the 3-D problem of Fig. 1, the computational domain contains both the external fluid and the solid fin. Thus, the solution of Eq. (8) is also required in order to obtain the complete temperature field. Instead of solving separately for the two entities (fluid and solid) and imposing the same heat flux at the interface solid–fluid, as a boundary condition, the solution is sought for the entire domain, simultaneously, with the same set of conservation equations, imposing zero velocities in the solid fin.

4. Experiments

An experimental rig was built in the laboratory to produce the necessary experimental data to validate the 2-D numerical optimization of non-finned arrangements, and to perform the experimental optimization of finned arrangements. Fig. 3 shows a schematic drawing of the experimental apparatus utilized in this study. A small scale wind tunnel was built with naval plywood to prevent deformations due to humidity. A test section was conceived in modular form as a drawer, to allow for testing many different arrangements configurations just by changing the test module shown in Fig. 3. The

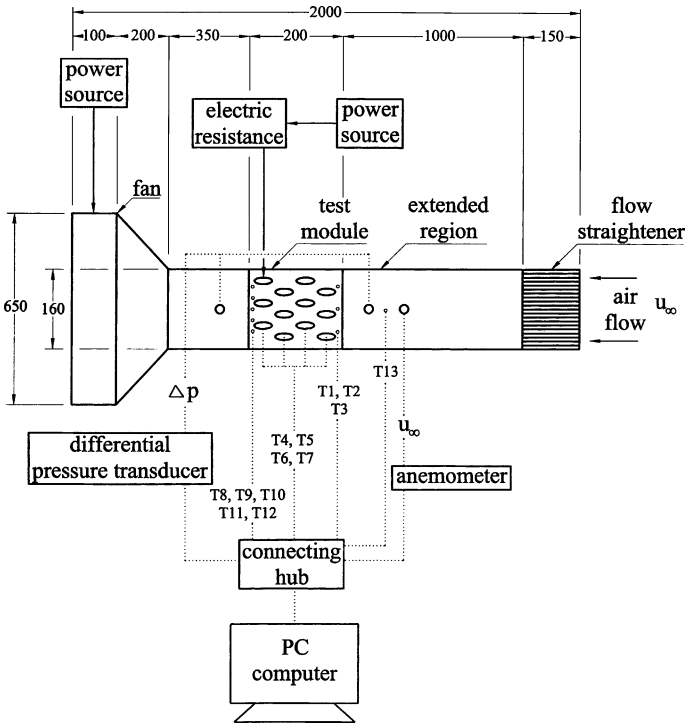

Fig. 3. Experimental apparatus.

internal dimensions of the test section are 175 mm × 161 mm × 152 mm. An extended region of 1000 mm was placed before the test section to allow the flow to fully develop before reaching the arrangement. A flow straightener was assembled with plastic straws at the entrance of the extended region with the purpose of laminarizing the flow as shown in Fig. 3.

The circular and elliptic tube arrangements were made from copper circular tubes with diameters of 15.875 mm (5/8 in.), 22.23 mm (7/8 in.), 25.4 mm (1 in.) and 28.58 mm (1 1/8 in.) which resulted in tubes with eccentricities $e = 1.0$, 0.6, 0.5 and 0.4, respectively, with a wall thickness of 0.79375 mm (1/32 in.) for all eccentricities. To make the elliptic arrangements, the circular tubes were conformed in the machine shop with an appropriately designed tool. All tubes had a length of 172 mm. Electric heaters were placed inside the tubes to simulate the heat flux originated from a hot fluid. All the arrangements had four rows in the direction of the external flow, as shown in Fig. 1. Twelve tubes were then assembled according to the design presented in Fig. 1, in a wooden drawer, which is the test module shown in Fig. 3. All the fins were made from aluminum plates with dimensions of 150 mm × 130 mm × 0.3 mm.

The electric heaters consisted of double step tubular electric resistances with 968 Ω, therefore with a maximum power dissipation of 50 W with 220 V. The electric heaters had a small enough diameter to be fitted into the copper tubes, and were fed with a variable voltage source (30 V, 1.4 A), in order to allow all arrangements under comparison to have the same power input.

Twelve high precision thermistors of type YSI 44004 (resistance 2250 Ω at 25 °C) were placed in each test module. All the thermistors were placed in the midplane between the side walls of the wind tunnel and at the midline of the elemental channels. Three thermistors were placed at the arrangement inlet (T1–T3), five at the outlet (T8–T12), and four at the tubes surfaces in one elemental channel (T4–T7). An additional thermistor (T13) was placed at the midpoint of the extended region to measure the non-disturbed free stream temperature. The thermistors at the inlet and outlet of the arrangement permitted the determination of the vertical variation of temperature in the arrangement. In all the tests performed, the vertical temperatures remained within a ±0.5 °C margin with respect to the average (vertical) temperatures calculated at the inlet and outlet. The thermistors at the tubes surfaces showed that the temperature difference between tubes in one elemental channel is negligible, namely, within a ±0.3 °C margin with respect to the average of the four thermistors. Finally, the additional thermistor placed at the extended region measured free stream temperatures within a ±0.5 °C margin with respect to the measured average arrangement inlet temperature, in all tests performed in this work.

The velocity measurements were taken with a vane-type digital anemometer, model HHF 300A (OMEGA Engineering, Inc.), which was placed at the extended flow region, as shown in Fig. 3. For the range of 0.1–35 m/s, the velocity bias limit is ±2.5% of the reading. The free stream velocity was varied between 0.1 and 1 m/s in this study. To allow for the continuous variation of the fan velocity, a variable power source was utilized with 30 V and a maximum current of 2 A.

The pressure drop measurements were taken with a pressure transducer, model PX137-0.3DV (OMEGA Engineering, Inc.), with a nominal range of (0–2068.5 Pa), which was connected to a digital pressure meter, model DP25B-S (OMEGA Engineering, Inc.). The differential pressure maximum bias limit is ±1% of the reading. The differential pressure measurements had the finality of measuring the pressure drop across each arrangement in all experiments, as shown in Fig. 3.

The experimental work involved the acquisition of temperature data in real time. This task was performed through the utilization of a computational data acquisition system which consisted of a virtual data logger AX5810 (User's manual [17]) and four multiplexers AX758 (User's manual [18]) which allowed for the sequential data acquisition from 64 channels at interval times of 1/256 s. All the data were processed by a suitable software application to convert the sensors signals in readable temperatures.

The thermistors were calibrated in the laboratory to determine the bias limits. The thermistors were immersed in a constant temperature bath maintained by a bath circulator, and a total of 64 temperature measurements were made at $20, 30, \ldots, 80$ °C. The largest standard deviation of these measurements was 0.0005 °C, and therefore the bias limit was set at ±0.001 °C for all thermistors; this bias limit is in agreement with the ±0.0003 °C of the same thermistors in a natural convection experiment [19] and with the ±0.0005 °C bias limit listed in an instrumentation handbook [20].

The objective of the experimental work was to evaluate the volumetric heat transfer density (or overall thermal conductance) of each tested arrangement by computing $\tilde{q}_*$ with Eq. (17) through direct measurements of $u_\infty(Re_L)$, and $\overline{T}_{out}$, $\overline{T}_w$ and $T_\infty(\bar{\theta}_{out})$. Five runs were conducted for each experiment. Steady-state conditions were reached after 3 h in all the experiments. The precision limit for each temperature point was computed as two times the standard deviation of the five runs [21]. It was verified that the precision limits of all variables involved in the calculation of $\tilde{q}_*$ were negligible in comparison to the precision limit of $\bar{\theta}_{out}$, therefore $P_{\tilde{q}_*} \cong P_{\bar{\theta}_{out}}$. The thermistors, anemometer, properties, and lengths bias limits were found negligible in comparison with the precision limit of $\tilde{q}_*$. As a result, the uncertainty of $\tilde{q}_*$ was calculated by

$$\frac{U_{\tilde{q}_*}}{\tilde{q}_*} = \left[\left(\frac{P_{\tilde{q}_*}}{\tilde{q}_*}\right)^2 + \left(\frac{B_{\tilde{q}_*}}{\tilde{q}_*}\right)^2\right]^{1/2} \cong \frac{P_{\bar{\theta}_{out}}}{\bar{\theta}_{out}} \tag{18}$$

where $P_{\bar{\theta}_{out}}$ is the precision limit of $\bar{\theta}_{out}$.

The tested arrangements had a total of 12 tubes placed inside the fixed volume LHW, with four tubes in each unit cell (four rows). For a particular tube and plate fin geometry, the tests started with an equilateral triangle configuration, which filled uniformly the fixed volume, with a resulting maximum dimensionless tube-to-tube spacing $S/2b = 1.5$. The spacing between tubes was then progressively reduced, i.e., $S/2b = 1.5$, 0.5, 0.25 and 0.1, and in this interval an optimal spacing was found such that $\tilde{q}_*$ was maximum. All the tested arrangements had the aspect ratio $L/2b = 8.52$.

Several free stream velocities set points were tested, such that $u_\infty = 0.1$, 0.13, 0.3, 0.65 and 1 m/s, corresponding to $Re_L = 852$, 1065, 2840, 5680 and 8520, respectively. The largest uncertainty calculated according to Eq. (18) in all tests was $U_{\tilde{q}_*}/\tilde{q}_* = 0.048$.

5. Results and discussion

The results obtained in this study are divided in two parts: (i) experimental validation of numerical optimization results for non-finned arrangements, and (ii) experimental optimization results for finned and non-finned arrangements.

For the first part, the non-linear system of finite element equations was solved by the Newton–Raphson method [15], to obtain the velocities and temperatures in the computational domain of Fig. 2. The dimensionless temperatures at the elemental channel outlet are then utilized to compute the dimensionless volumetric heat transfer density, $\tilde{q}_*$, defined by Eq. (17).

The numerical results obtained with Eq. (17) are expected to be more accurate than the results that would be obtained by computing the sum of heat fluxes at the tubes surfaces in the elemental channel. The reason is that the former are obtained from the finite element temperature solution, whereas the latter are obtained from temperature spatial derivatives which are computed from post-processing the finite element solution. It is well known that the numerical error in the derivative of the solution is larger than the numerical error in the solution itself.

To obtain accurate numerical results, several mesh-refinement tests were conducted. The monitored quantity was the dimensionless overall thermal conductance, computed with Eq. (17), according to the following criterion:

$$\varepsilon = |\tilde{q}_{*,j} - \tilde{q}_{*,j-1}|/|\tilde{q}_{*,j}| \leqslant 0.01 \tag{19}$$

where j is the mesh iteration index, i.e., as j increases the mesh is more refined. When the criterion is satisfied, the $j-1$ mesh is selected as the converged mesh.

The criterion defined by Eq. (19) was used to find the appropriate length to the extension domain defined in the unit cell of Fig. 2. An extra-length L had to be added to the computational domain, upstream and downstream of the unit cell to represent the actual flow, and satisfied Eq. (19), when compared to an extra-length $3L/2$. Non-regular meshes were utilized in the procedure, such that mesh-regions close to the tubes were more refined, where the highest gradients in the solution were expected. The last three mesh iterations had (a) 2730 nodes and 2508 elements, (b) 5460 nodes and 5180 elements, and (c) 5670 nodes and 5380 elements, with a relative error below 3% when (a) and (b) are compared, and below 1% when (b) and (c) are compared, according to Eq. (19). Therefore, for all cases the mesh was established to consist of 5460 nodes and 5180 elements.

The numerical results obtained with the finite element code are validated by direct comparison to experimental results obtained in the laboratory for circular and elliptic arrangements. According to Fig. 1 the dimensions of the fixed volume for the experimental optimization procedure were $L = 135.33$ mm, $H = 115.09$ mm, $W = 152$ mm, and $D = 2b = 15.875$ mm. All the arrangements had $N_{ec} = 6$ and $N = 4$, where N is the number of tubes in one unit cell.

The numerical and experimental optimization procedures followed the same steps. First, for a given eccentricity, the dimensionless overall thermal conductance, $\tilde{q}_*$, was computed with Eq. (17), for the range $0.1 \leqslant S/2b \leqslant 1.5$. The same procedure was repeated for $e = 0.45$, 0.5, 0.6 and 1. The numerical double optimization results for non-finned tubes ($\phi_f = 0$) with respect to tube-to-tube spacings and eccentricities are shown in Fig. 4, together with the corresponding experimental results, for $Re_L = 852$ and 1065. The direct comparison of $\tilde{q}_{*,max}$ obtained numerically and experimentally shows that the results are in good qualitative agreement. The agreement is remarkable if we consider that in the experiments the tested arrays had uniform heat flux, and were not large banks of cylinders. In the numerical simulations the domain was infinitely wider (i.e., no influence from the wind tunnel walls) and with isothermal tubes. However, it was observed by means of direct temperature measurements that the uniform wall heat flux experimental condition approximately reproduced the constant wall temperature condition used in the numerical simulations. For that, in one tube of the array, four thermistors were placed equally spaced on the tube surface around the two extremities and middle sections, resulting in a total of 12 thermistors. The test was repeated for different tubes in the experimental arrays. The measured temperature on the tube surface was within ±0.2 °C with respect to the average tube surface

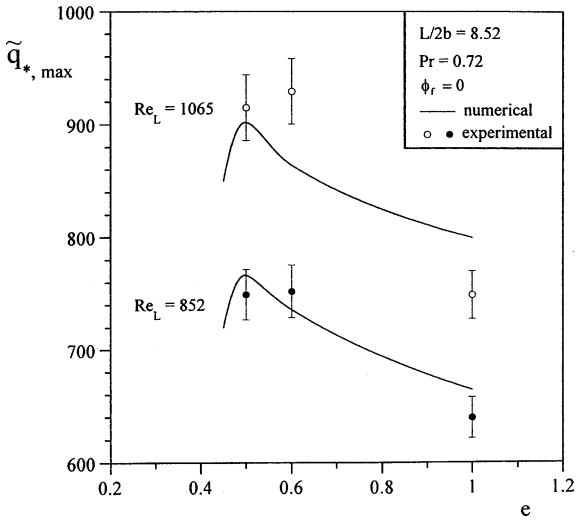

Fig. 4. Numerical and experimental optimization results for non-finned arrangements.

temperature, considering all tests performed. The optima are sharp, stressing their importance in actual engineering design. The optimal tube-to-tube spacings found numerically and experimentally for $Re_L = 852$ and 1065, were in the range $0.25 \leqslant (S/2b)_{opt} \leqslant 0.5$, for $0.45 \leqslant e \leqslant 1$.

As stated in Section 2, the governing equations are for the laminar regime. Therefore, the results of Fig. 4 were obtained for low Reynolds numbers, i.e., $Re_L = 852$ and 1065. For higher Reynolds numbers, convergence to numerical solutions becomes increasingly more difficult, indicating the flow is reaching a regime of transition to turbulence.

Pressure drop measurements were performed for all circular and elliptic arrangements under comparison. The measurements were conducted for non-finned ($\phi_f = 0$) and finned arrangements ($\phi_f = 0.006$), for all tested eccentricities, i.e., $e = 0.4$, 0.5, 0.6 and 1. For $Re_L = 2840$, 5680 and 8520 ($u_\infty = 0.3$, 0.65 and 1 m/s), the measured pressure drops were, respectively, 0.69, 0.92 and 1.15 Pa for ($\phi_f = 0$), and 0.92, 1.15 and 1.38 Pa for ($\phi_f = 0.006$), for all eccentricities. Hence, the pressure drop measurements demonstrate that the identical flow obstruction cross-sectional area criterion indeed leads to similar pressure drops for all tested eccentricities. The largest Reynolds number utilized in the experiments was $Re_L = 8520$ ($Re_D = 1000$), which corresponds to $Re_\delta = 3130$ (for $\delta = 49.7$ mm, $\phi_f = 0.006$), or $Re_\delta = 104$ (for $\delta = 1.65$ mm [3]), therefore smaller than the limit $Re_\delta \sim 200$ found by Bordalo and Saboya [3] where pressure drop differences were negligible with respect to changes in eccentricity. Consequently, all comparisons between circular and elliptic tubes performed in this study quantify the heat transfer gain in the most isolated way possible.

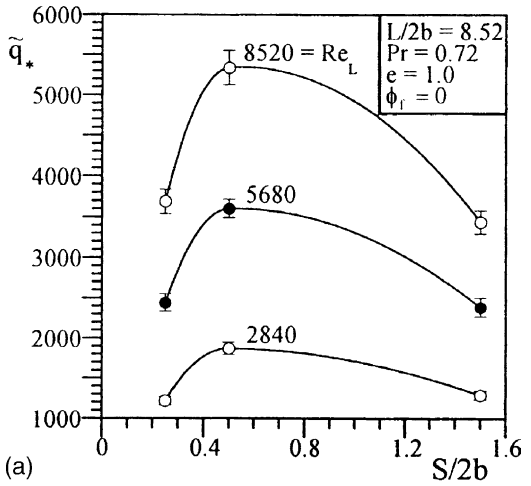

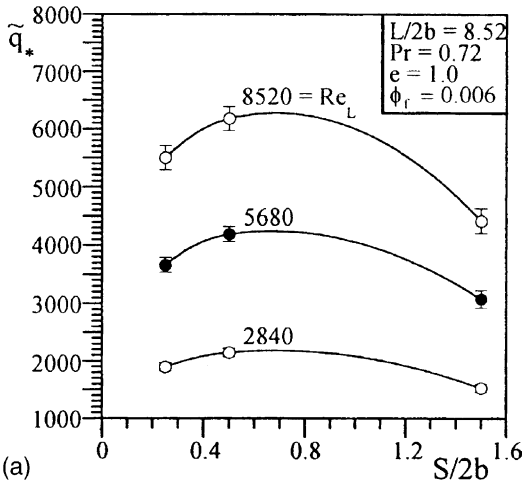

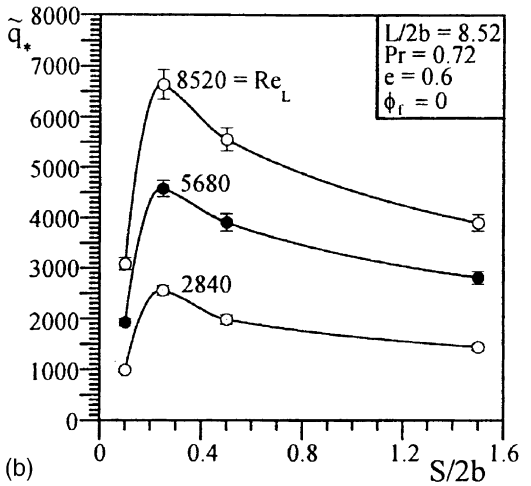

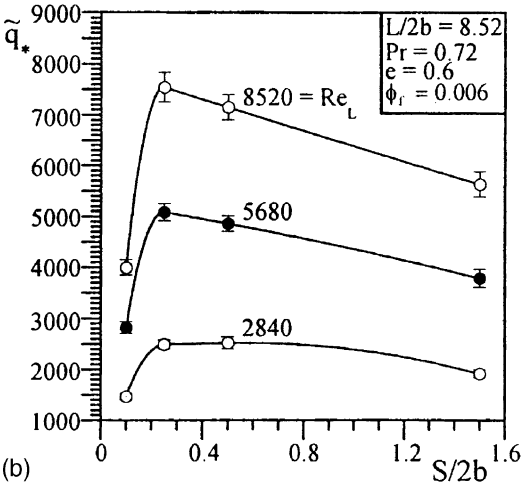

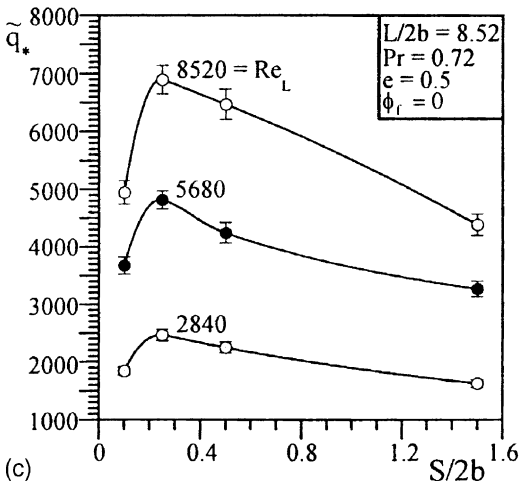

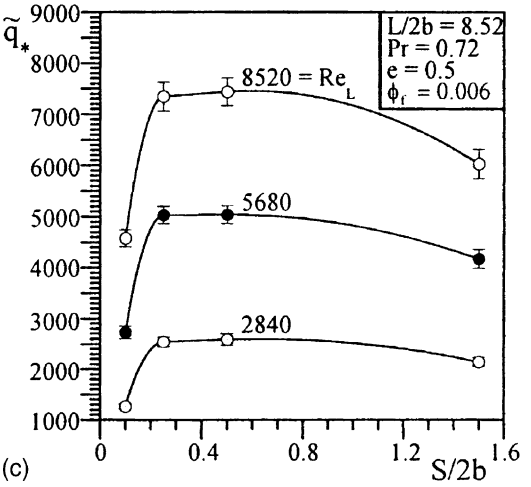

Fig. 5. Experimental optimization results for non-finned arrangements: (a) $e = 1$, (b) $e = 0.6$, and (c) $e = 0.5$.

Fig. 6. Experimental optimization results for finned arrangements: (a) $e = 1$, (b) $e = 0.6$, and (c) $e = 0.5$.

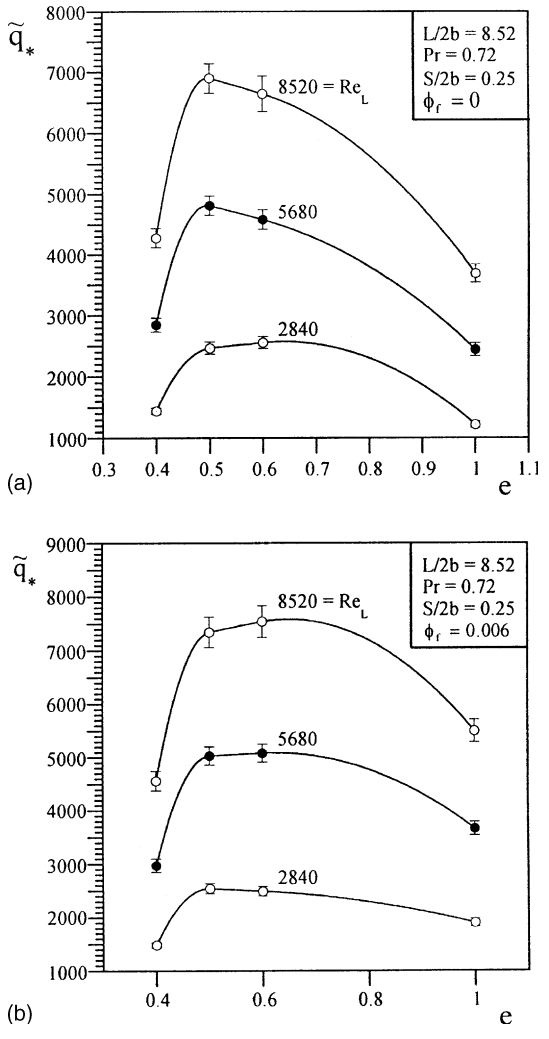

Fig. 7. The optimization of (a) non-finned and (b) finned arrangements with respect to eccentricity ($S/2b = 0.25$).

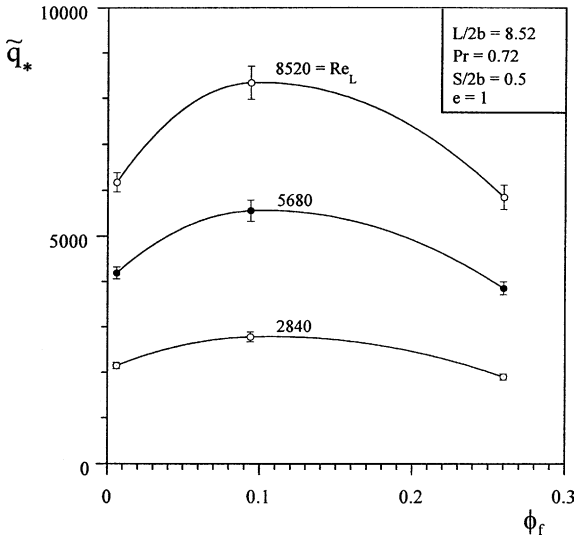

Fig. 8. Local optimization of finned circular arrangements with respect to fin-to-fin spacing ($S/2b = 0.5$).

The second part of this study presents experimental optimization results for a higher range of Reynolds numbers, i.e., for $Re_L = 2840$, 5680 and 8520. Figs. 5 and 6 show the experimental optimization of the tube-to-tube spacing, $S/2b$, for $e = 1$, 0.6 and 0.5, respectively, for non-finned and finned arrangements ($\phi_f = 0$ and 0.006).

The results indicate sharp optima for all eccentricities with respect to $S/2b$. The influence of the variation of Re_L is also investigated. As Re_L increases $\tilde{q}_*$ increases. The maximum is less pronounced for lower values of Re_L.

The experimental optimization procedure should continue with respect to eccentricity. However, a closer inspection of Figs. 5 and 6 show that for $e = 0.5$ and 0.6, $\tilde{q}_{*,max}$ with respect to $(S/2b)_{opt}$ is a little smaller for $e = 0.5$ than for $e = 0.6$, but within the uncertainty limits. Therefore $\tilde{q}_{*,max}$ for $(S/2b)_{opt}$ should be obtained also for a lower eccentricity value, e.g., $e = 0.4$, to find a global optimum with respect to $S/2b$ and e. Furthermore, it was observed that $(S/2b)_{opt} \cong 0.25$ both for $e = 0.5$ and 0.6 ($\phi_f = 0$ and $\phi_f = 0.006$). Therefore, in a search for global optima with respect to $S/2b$ and e, additional arrangements were built, with $S/2b = 0.25$ and $e = 0.4$, which allowed the determination of local optimal eccentricity for $S/2b = 0.25$ for $\phi_f = 0$ and 0.006, as shown in Fig. 7. These local optima results are a clear indication of a global optimal pair $(S/2b, e)_{opt}$ close to the results shown in Fig. 7.

Additionaly, Figs. 5–7 show that the optimal pair $(S/2b, e)_{opt} \cong (0.25, 0.5)$ is "robust" for a wide variation range of external flow conditions, i.e., for $Re_L =$ 2840, 5680 and 8520, which pinpoints a possible general optimal geometry worth to be furtherly investigated.

Fig. 8 shows the existence of a local optimal fin-to-fin spacing, ϕ_f, for $S/2b = 0.5$ and $e = 1$ (circular tubes). In all the experimental results shown in Figs. 5–8, it was observed that as Re_L increases $\tilde{q}_*$ increases, with sharper maxima occurring at higher Re_L.

From all numerical and experimental results obtained in this study, it is important to stress that a heat transfer gain of up to 20% was observed in the optimal elliptic arrangement with $e = 0.5$, as compared to the optimal circular one. The presented results are also an indication of the existence of global optima with respect to $S/2b$, e and ϕ_f, for maximum heat transfer.

6. Conclusions

In this paper, a theoretical, numerical and experimental study was conducted to demonstrate that non-finned and finned circular and elliptic tubes heat exchangers can be optimized for maximum heat transfer, under a fixed volume constraint. The internal geometric structure of the arrangements was optimized for maximum heat transfer. Better global performance is achieved when flow and heat transfer resistances are minimized together, i.e., when the imperfection is distributed in space optimally [1]. Optimal distribution of imperfection represents flow architecture, or constructal design.

The results were presented non-dimensionally to allow for general application to heat exchangers of the type treated in this study. A suitable equivalent pressure drop criterion permitted the comparison between circular and elliptic arrangements on a heat transfer basis in the most isolated way possible, for $Re_\delta < 200$ (criterion for $\delta = 1.65$ mm [3]). A heat transfer gain of up to 20% was observed in the optimal elliptic arrangement, as compared to the optimal circular one. For higher Re_δ (not treated in the present study), the difference of the pressure drops between elliptic and circular arrangements are not negligible, and the heat transfer gain, combined with the relative pressure drop reduction of up to 30% in favor of the elliptic configuration observed in previous studies [2,3], show that the finned elliptical arrangement has the potential for a considerably better overall performance than the traditional circular one.

Three degrees of freedom were investigated in the heat exchanger geometry, i.e., tube-to-tube spacing, eccentricity and fin-to-fin spacing. However, the experimental results did not cover all possible combinations of the three degrees of freedom in the variation ranges studied. Global optima were found with respect to tube-to-tube spacing and eccentricity. Regarding fin-to-fin spacing, local optima were found for a fixed tube-to-tube spacing ($S/2b = 0.5$) and eccentricity ($e = 1$). Therefore, the present results indicate the existence of global optima and motivate the development of a general numerical model such that optimal arrangements of finned tubes could be searched non-dimensionally with respect to all three geometric degrees of freedom simultaneously for maximum heat transfer. Such globally optimized configurations are expected to be of great importance for actual heat exchangers engineering design, and for the generation of optimal flow structures in general.

Acknowledgements

The authors acknowledge with gratitude the support of the Program of Human Resources for the Oil Sector and Natural Gas, of the Brazilian Oil National Agency PRH-ANP/MCT.

References

[1] A. Bejan, Shape and Structure, from Engineering to Nature, Cambridge University Press, Cambridge, UK, 2000.
[2] H. Brauer, Compact heat exchangers, Chem. Process Eng. (August) (1964) 451–460.
[3] S.N. Bordalo, F.E.M. Saboya, Pressure drop coefficients for elliptic and circular sections in one, two and three-row arrangements of plate fin and tube heat exchangers, J. Braz. Soc. Mech. Sci. XXI (4) (1999) 600–610.
[4] S.M. Saboya, F.E.M. Saboya, Experiments on elliptic sections in one and two-row arrangements of plate fin and tube heat exchangers, Exp. Thermal Fluid Sci. 24 (2001) 67–75.
[5] J.Y. Jang, J.Y. Yang, Experimental and 3-d numerical analysis of the thermal-hydraulic characteristics of elliptic finned-tube heat exchangers, Heat Transfer Eng. 19 (4) (1998) 55–67.
[6] L.A.O. Rocha, F.E.M. Saboya, J.V.C. Vargas, A comparative study of elliptical and circular sections in one and two-row tubes and plate fin heat exchangers, Int. J. Heat Fluid Flow 18 (1997) 247–252.
[7] F.E.M. Saboya, E.M. Sparrow, Experiments on a three-row fin and tube heat exchangers, J. Heat Transfer 98 (1976) 520–522.
[8] E.C. Rosman, P. Carajilescov, F.E.M. Saboya, Performance of tube of one and two-row tube and plate fin heat exchangers, J. Heat Transfer 106 (1984) 627–632.
[9] R.S. Matos, J.V.C. Vargas, T.A. Laursen, F.E.M. Saboya, Optimization study and heat transfer comparison of staggered circular and elliptic tubes in forced convection, Int. J. Heat Mass Transfer 20 (2001) 3953–3961.
[10] O.C. Zienkiewicz, R.L. Taylor, The Finite Element Method, vol. 1, McGraw-Hill, London, 1989 (Chapter 15).
[11] G. Stanescu, A.J. Fowler, A. Bejan, The optimal spacing of cylinders in free-stream cross-flow forced convection, Int. J. Heat Mass Transfer 39 (2) (1996) 311–317.
[12] A.J. Fowler, A. Bejan, Forced convection in banks of inclined cylinders at low Reynolds numbers, Int. J. Heat Fluid Flow 15 (1994) 90–99.
[13] A. Bejan, Convection Heat Transfer, 2nd ed., Wiley, New York, 1995 (Chapters 2–3).
[14] A.J. Fowler, G.A. Ledezma, A. Bejan, Optimal geometric arrangement of staggered plates in forced convection, Int. J. Heat Mass Transfer 40 (8) (1997) 1795–1805.
[15] J.N. Reddy, D.K. Gartling, The Finite Element Method in Heat Transfer and Fluid Dynamics, CRC Press, Boca Raton, FL, 1994 (Chapters 4–5).
[16] T.J.R. Hughes, A simple scheme for developing upwind finite elements, Int. J. Numer. Methods Eng. 12 (1978) 1359–1365.
[17] User's Manual, AX5810 Virtual Data Logger, AXIOM Technology Co., Ltd., Part No. 925810, Rev. 1A, Taiwan, 1992.

[18] User's Manual, AX758 16 Channel Relay Multiplexer, AXIOM Technology Co., Ltd., Part No. 92758, Rev. 2A, Taiwan, 1992.
[19] L. Howle, J. Georgiadis, R. Behringer, Shadowgraphic visualization of natural convection in rectangular-grid porous layers, ASME HTD 206 (1) (1992) 17–24.
[20] J. Dally, W.F. Riley, K.G. McConnell, Instrumentation for Engineering Measurements, Wiley, New York, 1993, p. 425.
[21] Editorial, Journal of heat transfer policy on reporting uncertainties in experimental measurements and results, ASME Journal of Heat Transfer 115 (1993) 5–6.